Chapter 2

Evolution of Longitudinal Structure Function F_L Using Taylor Series Expansion Method at Small-x

In this chapter, we study the behaviour of the longitudinal structure function F_L of proton from its QCD evolution equation in NNLO approximation at small-x. Here we use the Taylor series expansion method to solve the evolution equation. The solution of this equation provides the expressions for $t=\left[ln(\frac{Q^2}{\Lambda^2})\right]$- and x-evolution equations for the computation of the longitudinal structure function. Our calculated results are compared with the recent H1 [1–5], ZEUS [6] experimental data, results of Donnachie-Landshoff (DL) models [7] and the theoretical predictions of MSTW08 [8], CT10 [9], ABM11 [10], NNPDF2.3 [11, 12] parameterizations. We have also compared our x-evolution results with the gluon dominating F_L structure function obtained by Boroun et al. [13]. Our predicted results show good agreement with the recent data and related fit and can be described within the framework of pQCD.

2.1 Theory

At small values of x, the density of gluons in the proton is considerably larger than densities of quarks and antiquarks. Thus, at small-x the structure of proton is mainly described by the distribution of gluons only. At small-x ($x \leq 10^{-3}$) the gluon contribution to the F_L structure function dominates over the singlet and non-singlet contribu-

tion [14]. Now the QCD evolution equation for gluon dominating F_L structure function is given by [15]

$$\frac{\partial F_L^g(x,Q^2)}{\partial lnQ^2} = K_G(x,Q^2) \otimes F_L^g(x,Q^2). \tag{2.1}$$

Here $K_G(x,Q^2)$ is the gluon kernel known perturbatively up to the first few orders in $\alpha_s(Q^2)$. The symbol $\otimes$ represents the standard Mellin convolution and is given by

$$A(x) \otimes B(x) = \int_0^1 \frac{dy}{y} A(y) B\Big(\frac{x}{y}\Big). \tag{2.2}$$

The kernel $K_G(x,Q^2)$ can be written as

$$K_G(x,Q^2) = \frac{\alpha_s(Q^2)}{4\pi} K_G^0(x) + \Big(\frac{\alpha_s(Q^2)}{4\pi}\Big)^2 K_G^1(x) + \Big(\frac{\alpha_s(Q^2)}{4\pi}\Big)^3 K_G^2(x) \tag{2.3}$$

up to NNLO, where $K_G^0(x)$, $K_G^1(x)$ and $K_G^2(x)$ are the gluon splitting kernel [16, 17] in LO, NLO and NNLO respectively. The expressions for $K_G^0(x)$, $K_G^1(x)$ are defined in Appendix A. $K_G^2(x)$ is available in co-efficient function form in Refs. [18, 19] and its expression is given in Appendix A. Using all these and simplifying QCD evolution equations for the longitudinal structure function in LO, NLO and NNLO, we get

$$\frac{\partial F_L^g(x,t)}{\partial t} - \frac{\alpha_s(t)}{4\pi}\left[\frac{80}{9}\int_x^1 dw w^2(1-w) F_L^g\Big(\frac{x}{w},t\Big)\right] = 0, \tag{2.4}$$

$$\frac{\partial F_L^g(x,t)}{\partial t} - \frac{\alpha_s(t)}{4\pi}\left[\frac{80}{9}\int_x^1 dw w^2(1-w) F_L^g\Big(\frac{x}{w},t\Big)\right] - \Big(\frac{\alpha_s(t)}{4\pi}\Big)^2 I_1^G(x,t) = 0 \tag{2.5}$$

and

$$\frac{\partial F_L^g(x,t)}{\partial t} - \frac{\alpha_s(t)}{4\pi}\left[\frac{80}{9}\int_x^1 dw w^2(1-w) F_L^g\Big(\frac{x}{w},t\Big)\right] - \Big(\frac{\alpha_s(t)}{4\pi}\Big)^2 I_1^G(x,t) - \Big(\frac{\alpha_s(t)}{4\pi}\Big)^3 I_2^G(x,t) = 0, \tag{2.6}$$

where

$$I_1^G(x,t) = \frac{160}{9}\int_x^1 dw f(w) F_L^g\Big(\frac{x}{w},t\Big) \tag{2.7}$$

and

$$I_2^G(x,t) = \int_x^1 dw K_G^2(w) F_L^g\Big(\frac{x}{w},t\Big). \tag{2.8}$$

Here $t = ln\frac{Q^2}{\Lambda^2}$, Λ is the QCD cut-off parameter and the function $f(w)$ is defined in Appendix A. The strong coupling constant in higher order has the form [20, 21]

$$\alpha_s(t) = \frac{4\pi}{\beta_0 t}\Big[1 - \frac{\beta_1}{\beta_0^2}\frac{lnt}{t} + \frac{1}{\beta_0^3 t^2}\Big\{\frac{\beta_1^2}{\beta_0}(ln^2 t - lnt - 1) + \beta_2\Big\} + O\Big(\frac{1}{t^3}\Big)\Big], \tag{2.9}$$

where

$$\beta_0 = 11 - \frac{2}{3}N_f, \tag{2.10}$$

$$\beta_1 = 102 - \frac{38}{3}N_f \tag{2.11}$$

and

$$\beta_2 = \frac{2857}{2} - \frac{5033}{18}N_f + \frac{325}{54}N_f^2 \tag{2.12}$$

are the one loop, two loop and three loop correction to the QCD β-function, N_f being the number of flavours. Here we take $N_f = 4$.

Equations (2.4), (2.5) and (2.6) can be solved by Taylor series expansion method as described in ref. [22, 23]. Considering the variable $u = 1 - w$, and since $x < w < 1$, we have $0 < u < 1 - w$; so the series $\frac{x}{w} = \frac{x}{1-u}$ is convergent for $|u| < 1$ and using the Taylor expansion method and neglecting the higher order terms, $F_L^g\Big(\frac{x}{w},t\Big)$ can be approximated for small-x as

$$\begin{aligned} F_L^g\Big(\frac{x}{w},t\Big) &= F_L^g\Big(x+\frac{xu}{1-u},t\Big) \\ &= F_L^g(x,t)+\frac{xu}{1-u}\frac{\partial F_L^g(x,t)}{\partial x}. \end{aligned} \tag{2.13}$$

Using (2.13) in equations (2.4), (2.5) and (2.6) and performing u-integrations we get

$$\frac{\partial F_L^g(x,t)}{\partial t}-\frac{1}{t}\Big[A_1(x)\frac{\partial F_L^g(x,t)}{\partial x}+B_1(x)F_L^g(x,t)\Big]=0, \tag{2.14}$$

$$\frac{\partial F_L^g(x,t)}{\partial t}-\frac{1}{t}\Big(1-b\frac{lnt}{t}\Big)\Big[A_2(x)\frac{\partial F_L^g(x,t)}{\partial x}+B_2(x)F_L^g(x,t)\Big]=0 \tag{2.15}$$

and

$$\begin{aligned} &\frac{\partial F_L^g(x,t)}{\partial t}-\frac{1}{t}\Big(1-b\frac{lnt}{t}+\frac{b^2}{t^2}(ln^2t-lnt-1)+\frac{c}{t^2}\Big) \\ &\qquad\Big[A_3(x)\frac{\partial F_L^g(x,t)}{\partial x}+B_3(x)F_L^g(x,t)\Big]=0, \end{aligned} \tag{2.16}$$

where

$$A_1(x)=\frac{1}{\beta_0}P_2(x),\quad B_1(x)=\frac{1}{\beta_0}P_1(x),\quad A_2(x)=\frac{1}{\beta_0}(P_2(x)+T_0Q_2(x)),$$

$$B_2(x)=\frac{1}{\beta_0}(P_1(x)+T_0Q_1(x)),\quad A_3(x)=\frac{1}{\beta_0}(P_2(x)+T_0Q_2(x)+T_1R_2(x)),$$

$$B_3(x)=\frac{1}{\beta_0}(P_1(x)+T_0Q_1(x)+T_1R_1(x)),$$

$$P_1(x)=\frac{80}{9}\Big(\frac{1}{12}-\frac{x^3}{3}+\frac{x^4}{4}\Big),\qquad P_2(x)=\frac{80}{9}x\Big(\frac{1}{12}-\frac{x^2}{2}+\frac{2x^3}{3}-\frac{x^4}{4}\Big),$$

$$Q_1(x) = \frac{160}{9}\int_x^1 f(w)dw, \qquad Q_2(x) = \frac{160}{9}x\int_x^1 \frac{(1-w)}{w}f(w)dw,$$

$$R_1(x) = \int_x^1 K_G^2(w)dw, \qquad R_2(x) = x\int_x^1 \frac{(1-w)}{w}K_G^2(w)dw,$$

$$b = \frac{\beta_1}{\beta_0^2} \qquad \text{and} \qquad c = \frac{\beta_2}{\beta_0^3}.$$

Here we consider two numerical parameters T_0 and T_1, such that $T^2(t) = T_0.T(t)$ and $T^3(t) = T_1.T(t)$ with $T(t) = \frac{\alpha_s(t)}{4\pi}$. These numerical parameters are obtained for a particular range of Q^2 under study. As described in ref. [23], these two parameters are chosen in such a way that the difference between $T^2(t)$, $T_0.T(t)$ and $T^3(t)$, $T_1.T(t)$ are negligible in our required range. This is explained in figure 2.1. Here, we have considered the values of $T_0 = 0.0278$ and $T_1 = 0.000892$ within the range $1.5 \leq Q^2 \leq 800GeV^2$.

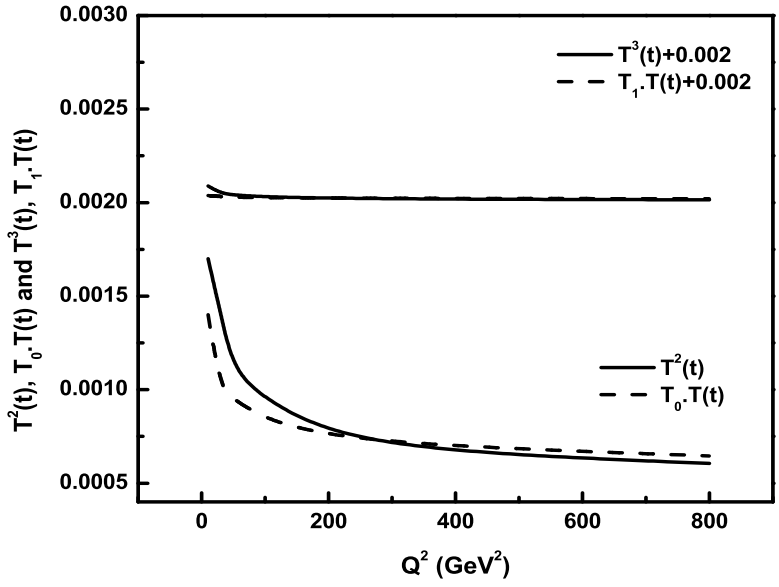

Figure 2.1: $T^2(t) = T_0.T(t)$ and $T^3(t) = T_1.T(t)$ versus $Q^2(GeV^2)$.

The general solution of equation (2.14) is $F(U,V)=0$, where $F(U,V)$ is an arbitrary function [22]. Now, $U(x,t,F_L^g)=C_1$ and $V(x,t,F_L^g)=C_2$ with C_1 and C_2, two constants, form a solution of the Lagrange's equation

$$\frac{dx}{A_1(x)}=-\frac{dt}{t}=-\frac{dF_L^g(x,t)}{B_1(x)F_L^g(x,t)} \tag{2.17}$$

from which we obtain

$$U(x,t,F_L^g)=t\cdot\exp\left[\int\frac{dx}{A_1(x)}\right] \tag{2.18}$$

and

$$V(x,t,F_L^g)=F_L^g(x,t)\cdot\exp\left[\int\frac{B_1(x)}{A_1(x)}dx\right]. \tag{2.19}$$

It thus has no unique solution. The simplest possibility is that a linear combination of U and V is to satisfy $F(U,V)=0$ so that $\alpha\cdot U+\beta\cdot V=0$, where α and β are arbitrary constants [22]. This combination gives

$$F_L^g(x,t)=-\Big(\frac{\alpha}{\beta}\Big)\cdot t\cdot\exp\left[\int\Big(\frac{1}{A_1(x)}-\frac{B_1(x)}{A_1(x)}\Big)dx\right]. \tag{2.20}$$

Now defining

$$F_L^g(x,t_0)=-\Big(\frac{\alpha}{\beta}\Big)\cdot t_0\cdot\exp\left[\int\Big(\frac{1}{A_1(x)}-\frac{B_1(x)}{A_1(x)}\Big)dx\right]$$

at $t=t_0$, where $t_0=ln\Big(\frac{Q_0^2}{\Lambda^2}\Big)$ at any lower value $Q=Q_0$, we get from equation (2.20)

$$F_L^g(x,t)=F_L^g(x,t_0)\Big(\frac{t}{t_0}\Big). \tag{2.21}$$

Again defining

$$F_L^g(x_0,t)=-\Big(\frac{\alpha}{\beta}\Big)\cdot t\cdot\exp\left[\int\Big(\frac{1}{A_1(x)}-\frac{B_1(x)}{A_1(x)}\Big)dx\right]_{x=x_0},$$

at any higher values of $x = x_0$, we obtain from equation (2.20)

$$F_L^g(x,t) = F_L^g(x_0,t)\exp\left[\int_{x_0}^{x}\Big(\frac{1}{A_1(x)} - \frac{B_1(x)}{A_1(x)}\Big)dx\right]. \tag{2.22}$$

Equations (2.21) and (2.22) give the t- and x-evolutions of longitudinal structure function F_L^g in LO respectively. Similarly, from equations (2.15) and (2.16), we obtain the t- and x-evolutions for F_L structure function in NLO and NNLO as

$$F_L^g(x,t) = F_L^g(x,t_0)\frac{t^{(1+b/t)}}{t_0^{(1+b/t_0)}}\exp\left[b\Big(\frac{1}{t} - \frac{1}{t_0}\Big)\right], \tag{2.23}$$

$$F_L^g(x,t) = F_L^g(x_0,t)\exp\left[\int_{x_0}^{x}\Big(\frac{1}{A_2(x)} - \frac{B_2(x)}{A_2(x)}\Big)dx\right] \tag{2.24}$$

and

$$F_L^g(x,t) = F_L^g(x,t_0)\frac{t^{(1+b/t)}}{t_0^{(1+b/t_0)}}\exp\left[\begin{array}{c} b\Big(\frac{1}{t} - \frac{1}{t_0}\Big) + \Big(\frac{b^2}{2} - \frac{c}{2}\Big)\Big(\frac{1}{t^2} - \frac{1}{t_0^2}\Big) \\ -\frac{b^2}{2}\Big(\frac{ln^2 t}{t^2} - \frac{ln^2 t_0}{t_0^2}\Big) \end{array}\right], \tag{2.25}$$

$$F_L^g(x,t) = F_L^g(x_0,t)\exp\left[\int_{x_0}^{x}\Big(\frac{1}{A_3(x)} - \frac{B_3(x)}{A_3(x)}\Big)dx\right] \tag{2.26}$$

respectively.

In our calculations, we used up to first order term $O(x)$ in Taylor expansion of $F_L^g\Big(\frac{x}{w},t\Big)$ and neglecting the higher order terms in small-x approximation. Now instead of neglecting the higher order terms $O(x^2)$ from the Taylor expansion series let us retain the second order term and neglecting the higher order terms $O(x^3)$, $F_L^g\Big(\frac{x}{w},t\Big)$ can then be approximated as

$$F_L^g\Big(\frac{x}{w},t\Big) \cong F_L^g(x,t) + \frac{xu}{1-u}\frac{\partial F_L^g(x,t)}{\partial x} + \frac{1}{2}\Big(\frac{xu}{1-u}\Big)^2\ \frac{\partial^2 F_L^g(x,t)}{\partial x^2}, \tag{2.27}$$

which gives from equation (2.4)

$$\frac{\partial F_L^g(x,t)}{\partial t} - \frac{1}{t}\Big[B_1(x)F_L^g(x,t) + A_1(x)\frac{\partial F_L^g(x,t)}{\partial x} + C_1(x)\frac{\partial^2 F_L^g(x,t)}{\partial x^2}\Big] = 0, \qquad (2.28)$$

where $C_1(x) = \frac{1}{\beta_0}\Big(\frac{x^2}{8} - \frac{x^3}{2} + \frac{3x^4}{4} - \frac{x^5}{2} + \frac{x^6}{8}\Big)$. $A_1(x)$ and $B_1(x)$ are given earlier.

The equation (2.28) is a second order partial differential equation and this can be solved by Monges method [24]. According to this method, the solution of second order partial differential equation

$$Rr + Ss + Tt = V \qquad (2.29)$$

can be obtained from the subsidiary equations

$$Rdy^2 + Sdxdy + Tdx^2 = 0 \qquad (2.30)$$

and

$$Rdpdy + Sdqdx - Vdxdy = 0, \qquad (2.31)$$

where R, S, T and V are functions of x, y, z, p and q. Here z, p, q, r, s and t are defined as follows

$$z = z(x,y) = F_L^g(x,t), \quad p = \frac{\partial z}{\partial x}, \quad q = \frac{\partial z}{\partial y}, \quad r = \frac{\partial^2 z}{\partial x^2} = \frac{\partial p}{\partial x},$$

$$s = \frac{\partial^2 z}{\partial x \partial y} = \frac{\partial p}{\partial y} = \frac{\partial q}{\partial x} \qquad \text{and} \qquad t = \frac{\partial^2 z}{\partial y^2} = \frac{\partial q}{\partial y}.$$

Comparing equations (2.28) and (2.29) we get

$$R = C_1(x), \quad S = 0, \quad T = 0 \quad \text{and}$$

$$V = t\frac{\partial F_L^g(x,t)}{\partial t} - A_1(x)\frac{\partial F_L^g(x,t)}{\partial x} - B_1(x)F_L^g(x,t).$$

Substituting the values of R, S, T and V in subsidiary equations (2.30) and (2.31) we ultimately obtain $V = 0$, which gives

$$\frac{\partial F_L^g(x,t)}{\partial t} - \frac{1}{t}\Big[A_1(x)\frac{\partial F_L^g(x,t)}{\partial x} + B_1(x)F_L^g(x,t)\Big] = 0, \qquad (2.32)$$

which is exactly same as the equation (2.14). Similarly, the other two equations (2.15) and (2.16) become same when we include the second order term in the Taylor expansion series. Thus it is clear that the inclusion of the second order term does not modify the solutions of the evolution equations. Similarly, if one introduce more higher order terms in Taylor expansion series, then for these cases also the term can be neglected due to smaller values of x [25, 26].

Thus we have obtained an analytical expression for the t- and x-evolutions of longitudinal structure function F_L^g. From the final expressions (2.21), (2.23) and (2.25), it is observed that our results, i.e., the t-evolutions depend upon the expressions of $\alpha_s(t)$ only. From these expressions we can easily calculate the t-evolutions of F_L^g by taking an input distribution at a given value of Q_0^2. The x-evolutions of F_L^g is determined from the expressions (2.22), (2.24) and (2.26) by taking an input distribution at a given value of x_0. Here, we have calculated the x-evolution up to NLO only. Due to the unavailability of the evolution kernel at NNLO we are unable to calculate the same at this order. But the co-efficient function and splitting function of quarks and gluon are available up to NNLO. So, we have calculated the structure function up to NLO in this chapter and up to NNLO in chapter 4 and 5. In chapter 4 and 5, we have calculated the structure function using the QCD evolution equation in terms of co-efficient function and splitting function of quarks and gluon and the details are described in the respective chapter.

2.2 Results and Discussions

Using the simple analytical expressions (2.21), (2.22), (2.23), (2.24) and (2.25), we have calculated the the gluon dominating longitudinal structure function F_L^g at small-x in leading, next-to-leading and next-to-next-to-leading orders. The obtained results are compared with the experimental data taken by H1 [1–5] and ZEUS collaboration [6], results of the Donnachie-Landshoff (DL) model [7] and the theoretical predictions from

MSTW08 [8], CT10 [9], ABM11 [10], NNPDF2.3 [11, 12] parameterizations. In H1 2001 data [2], the structure functions are measured in the kinematic range $1.5 \leq Q^2 \leq 150GeV^2$ and $3 \times 10^{-5} \leq x \leq 0.2$, for H1 2007 data [3,4], range is $2.5 \leq Q^2 \leq 25GeV^2$ and $5 \times 10^{-5} \leq x \leq 0.12$, for H1 2011 data [1], range is $1.5 \leq Q^2 \leq 120GeV^2$ and $2.9 \times 10^{-5} \leq x \leq 0.01$, for H1 2014 data [5], range is $35 \leq Q^2 \leq 800GeV^2$ and $6.5 \times 10^{-4} \leq x \leq 0.65$ and for ZEUS 2009 data [6], range is $20 < Q^2 < 130GeV^2$ and $5 \times 10^{-4} < x < 0.07$ respectively.

DL model [7] is based on dipole picture with a soft and a hard pomeron, large dipole couples to the soft pomeron and small dipole couples to the hard pomeron. The parameters in the model are fixed by proton-proton scattering data and proton structure function F_2^p data. The authors derived a good numerical fit to the output of the DGLAP evolution for the small-x behaviour of the gluon distribution function which is valid for Q^2 between 5 and $500GeV^2$. Here, they fitted their parameters with the H1 data sets [2]. The gluon distribution here is mainly dominated by the hard pomeron at small-x and for all Q^2. This not only describes the DGLAP evolution of hard part of the F_2, but also the longitudinal structure function. The MSTW08 PDFs [8] include updated LO, NLO and NNLO parton distribution functions determined from global analysis of hard-scattering data within the standard framework of leading-twist fixed-order collinear factorisation in the $\overline{MS}$ scheme. These parton distributions are a major update to the previously available MRST sets [27–29] and incorporate the maximum amount of information from DIS and other hard-scattering data. The CT10 PDFs of the proton describes theoretical advancements in the global QCD analysis that was used to produce the previous CTEQ6.6 [30] and CT09 [31] PDFs. This analysis includes the most recent collider data from deep-inelastic scattering, vector boson production, and single-inclusive jet production [9]. In CT10 PDFs the combined H1/ZEUS data [32] sets for DIS at HERA is also included. The ABM11 PDF fit is based on the world data for deep-inelastic scattering, fixed-target data for the Drell-Yan process and also

includes data from the LHC for the Drell-Yan process [10]. The NNPDF2.3 PDF fit, is the most accurate determination to date from the NNPDF family, and it supersedes previous existing sets. It differs from the NNPDF2.1 set because of the inclusion of LHC data [11].

Here, the proton longitudinal structure function, measured in the range $5 \leq Q^2 \leq 800GeV^2$ and $10^{-4} \leq x \leq 10^{-1}$, have been used for our analysis. The value of y used is greater than or equal to 0.5, as from this value onwards the contribution of F_L structure function is significant towards the total cross section [33]. The average values of Λ in our calculation is $0.22GeV$. In figure 2.2, F_L structure function is plotted against Q^2 for different values of x in comparison with the H1, ZEUS data and results of DL model. In figure 2.3, F_L structure function is plotted against x for different values of Q^2 in comparison with the H1, ZEUS data and the results of DL model. In figure 2.4, F_L structure function is plotted against x for different values of Q^2 in comparison with the H1, ZEUS data and the theoretical prediction of MSTW08. In figure 2.5, F_L structure function is plotted against x for different values of Q^2 in comparison with the H1, ZEUS data and theoretical prediction of CT10. Figures 2.6 and 2.7 describe our x-evolution results in comparison with the H1, ZEUS data and theoretical predictions of ABM11 and NNPDF2.3. The vertical error bars in all the plots are both statistical and systematic error for both H1 and ZEUS data. In all the graphs, the data points at lowest Q^2 values are taken as input point for t-evolution graphs and data points at highest x values are taken as input points for x-evolution graphs. To confirm that in spite of the large uncertainty in the experimental data, our results are in better agreement with the data, we add DL model results and the theoretical prediction of different parameterizations in all the figures.

It is observed from the t-evolution graphs that, our result shows good agreement with that of H1 and ZEUS data, i.e., with respect to the experimental data our result shows increasing behaviour with increasing values of Q^2. It is seen from the figure

2.2 that, our plots are in good agreement with DL model fit also and as the energy scale becomes larger, the agreement is better. But, at intermediate energy scale the agreement is not so good, the reason for this is that the DL model approach comes from a BFKL like evolution equation [7] and the Q^2-evolution in that case is somewhat different from a DGLAP approach. In all the cases, our calculated F_L structure function in LO, NLO and NNLO increase with the values of Q^2 in the given range like the results of DL model as expected from QCD. At small-x, F_L increases with Q^2 as we resolve increasing numbers of soft partons with increasing Q^2 [34]. The x-evolution results also show compatibility with the experimental data, model fit and the theoretical predictions of different parameterizations which are depicted in figure 2.3 to figure 2.7. Here the calculated values of F_L^g structure function increase with the decreasing x values. In case of the x-evolution results described in figure 2.3 to figure 2.7, the behaviour of LO, NLO curves are slightly different as we have considered the input point from different parameterizations. The behaviour of LO, NLO and NNLO curves in both the t- and x-evolutions of F_L^g structure function are different (i.e., sometimes NLO results overestimate LO prediction and vice versa) and this behaviour of the curves depend only on the expressions used for calculation of the structure function. Moreover, with reference to some recent papers [13, 35–37], we can say that the behaviour of the LO, NLO, NNLO curves depend only on the applied method. In all the figures, in spite of large uncertainty of the experimental data, all the plots show good agreement with the model fit and theoretical predictions of the parameterizations. It is observed from the x-evolution graphs that, our results show good agreement with the model fit and parameterizations and as the energy scale becomes larger, the agreement is better. In all our results for x-evolutions, we observe that the differences between LO and NLO results are extremely small and our NLO results are in better agreement with the data and fit. Moreover, in case of t-evolution the NLO and NNLO curves are almost overlapping with increasing values of Q^2 and our NNLO results are in better agreement

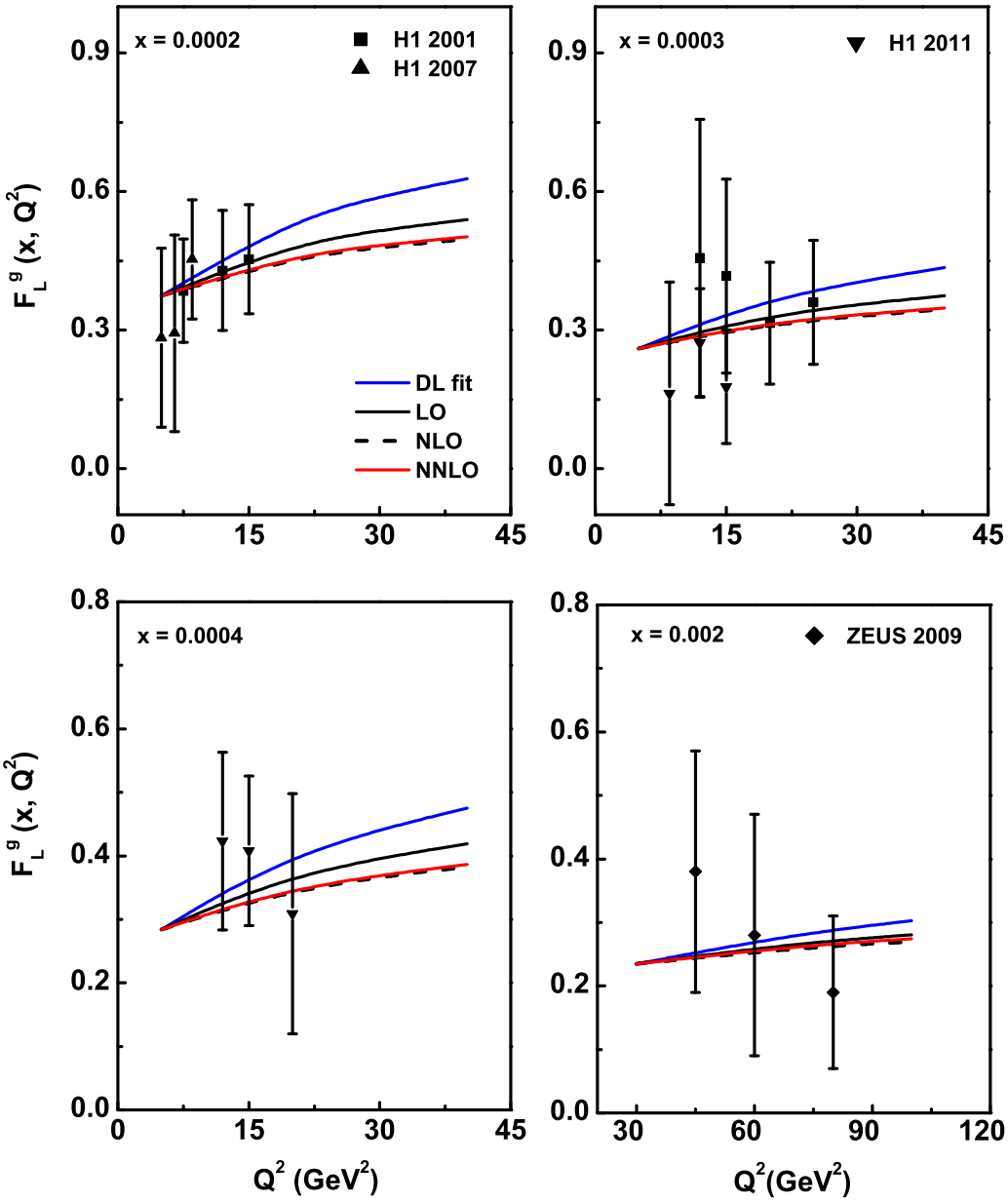

Figure 2.2: t-evolution results of F_L^g structure function up to NNLO using Taylor expansion method in comparison with the H1, ZEUS data and results of DL model.

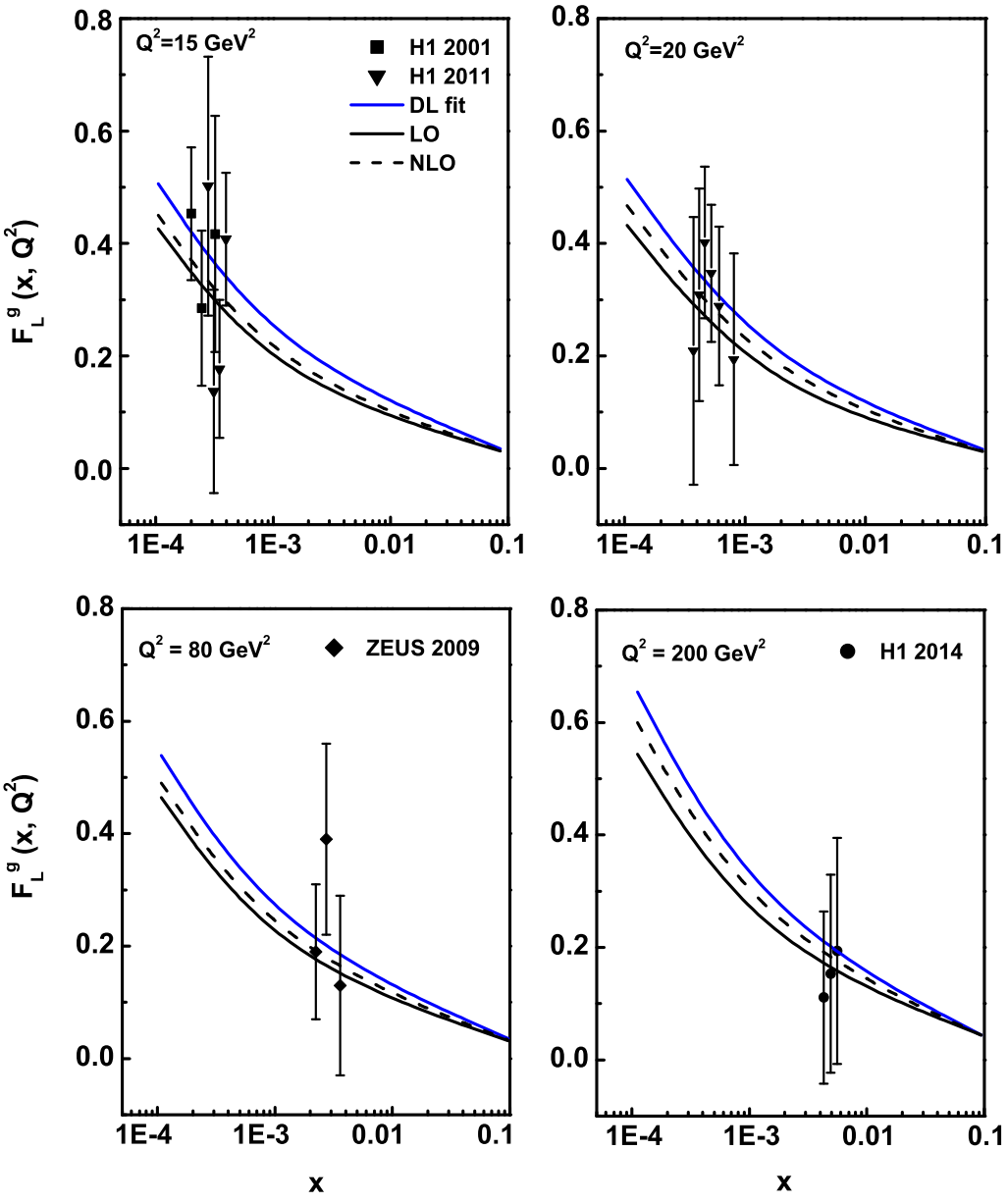

Figure 2.3: x-evolution results of F_L^g structure function up to NLO using Taylor expansion method in comparison with the H1, ZEUS data and results of DL model.

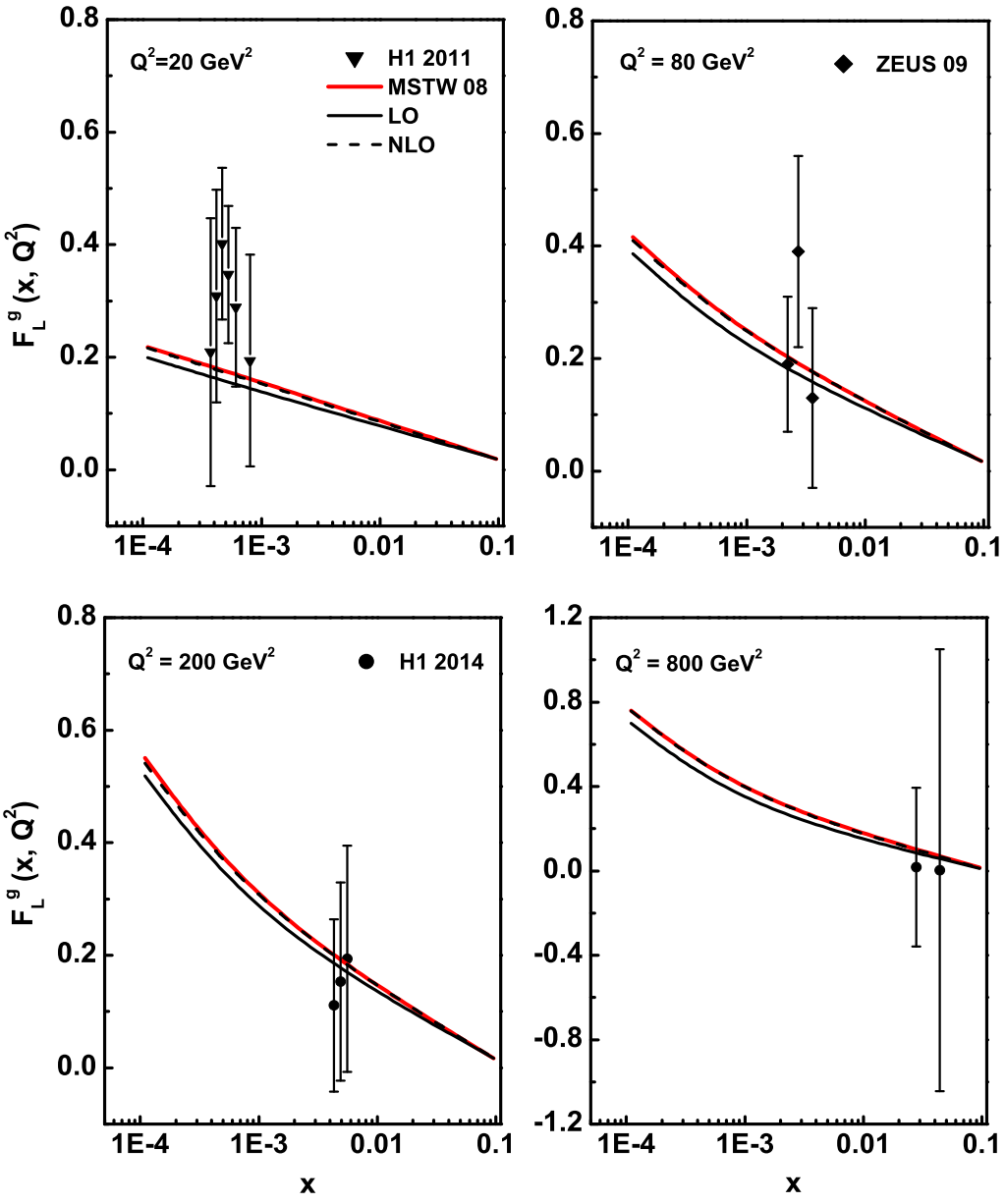

Figure 2.4: x-evolution results of F_L^g structure function up to NLO using Taylor expansion method in comparison with the H1, ZEUS data and the theoretical prediction of MSTW08.

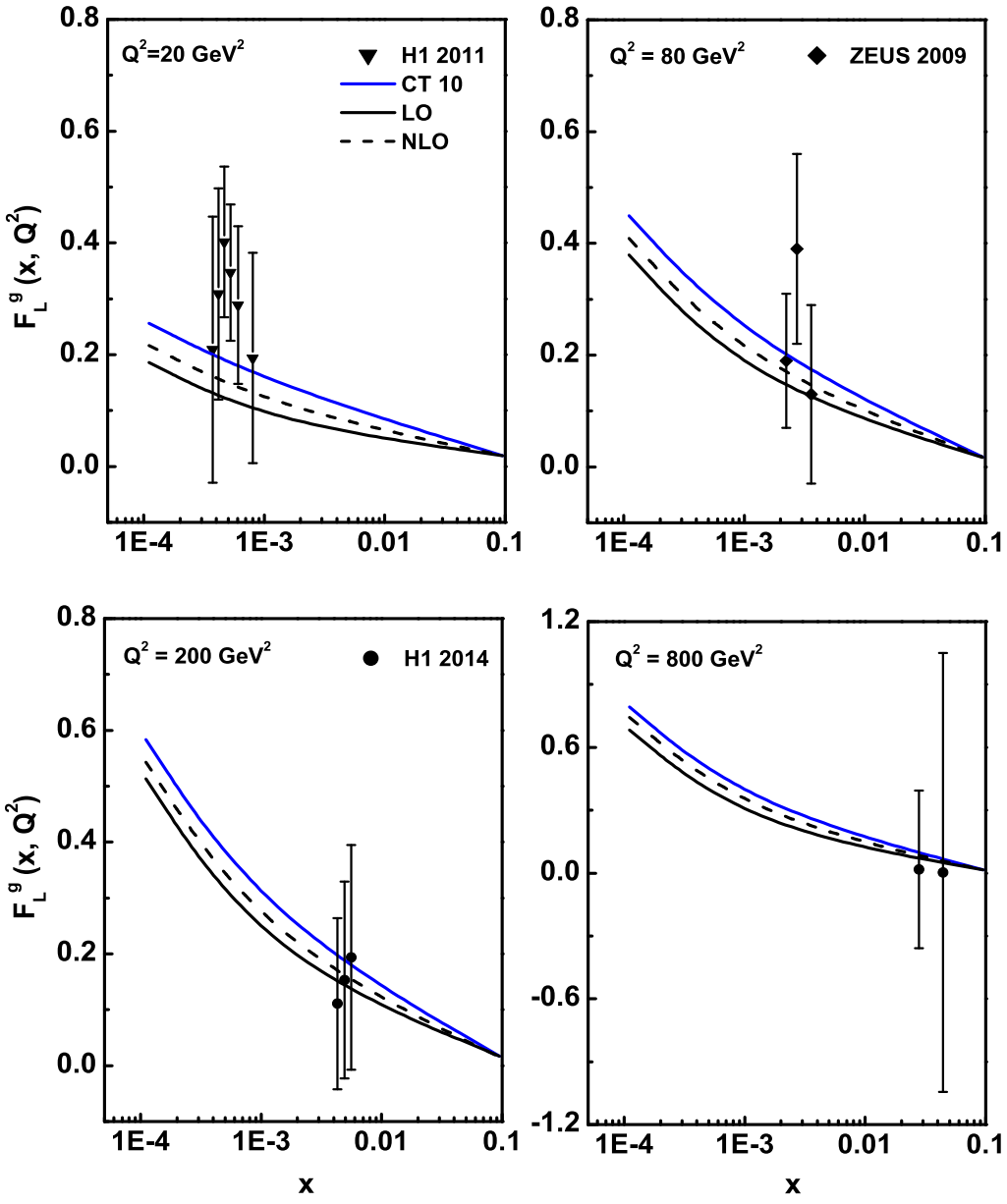

Figure 2.5: x-evolution results of F_L^g structure function up to NLO using Taylor expansion method in comparison with the H1, ZEUS data and the theoretical prediction of CT10.

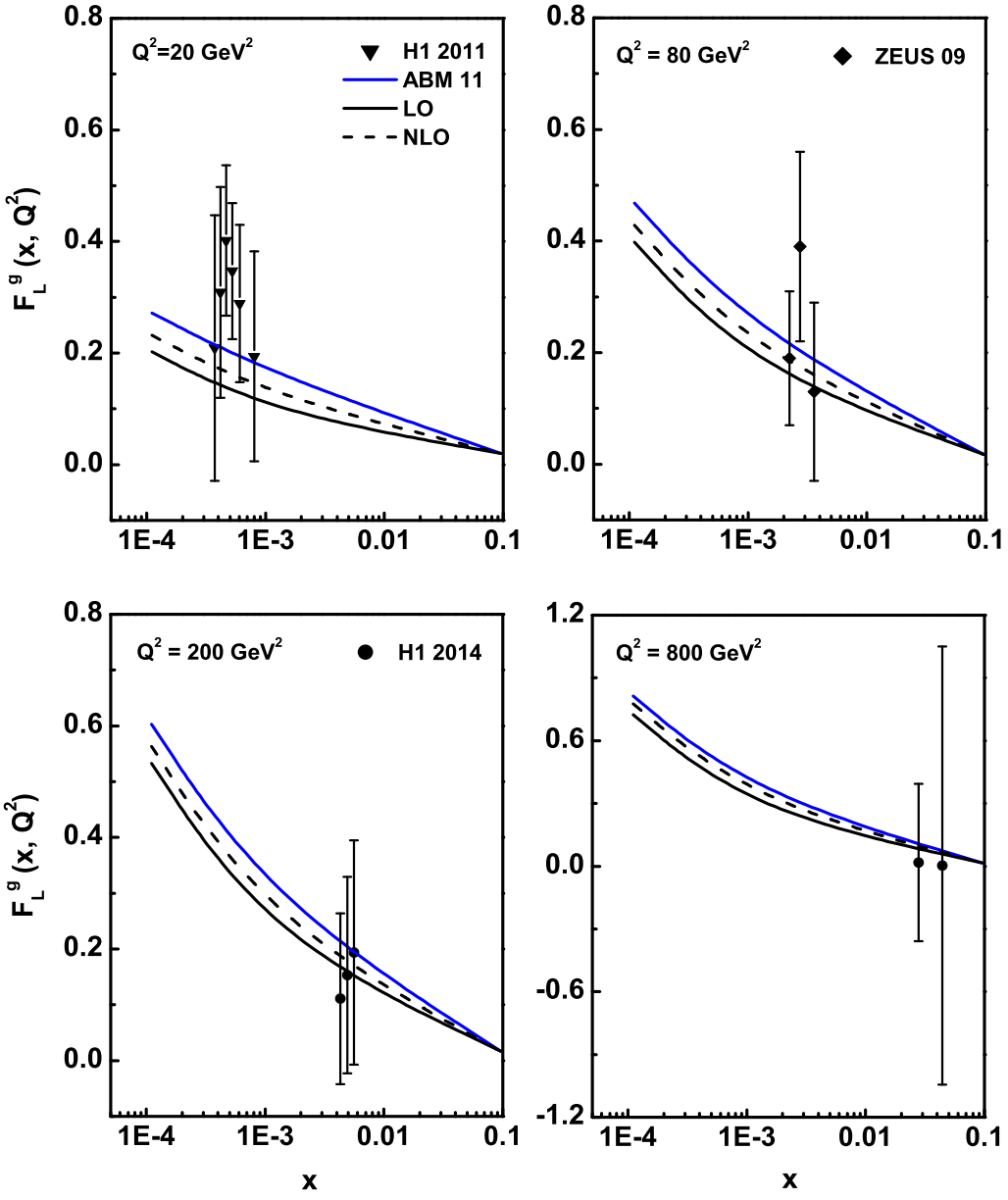

Figure 2.6: x-evolution results of F_L^g structure function up to NLO using Taylor expansion method in comparison with the H1, ZEUS data and the theoretical prediction of ABM11.

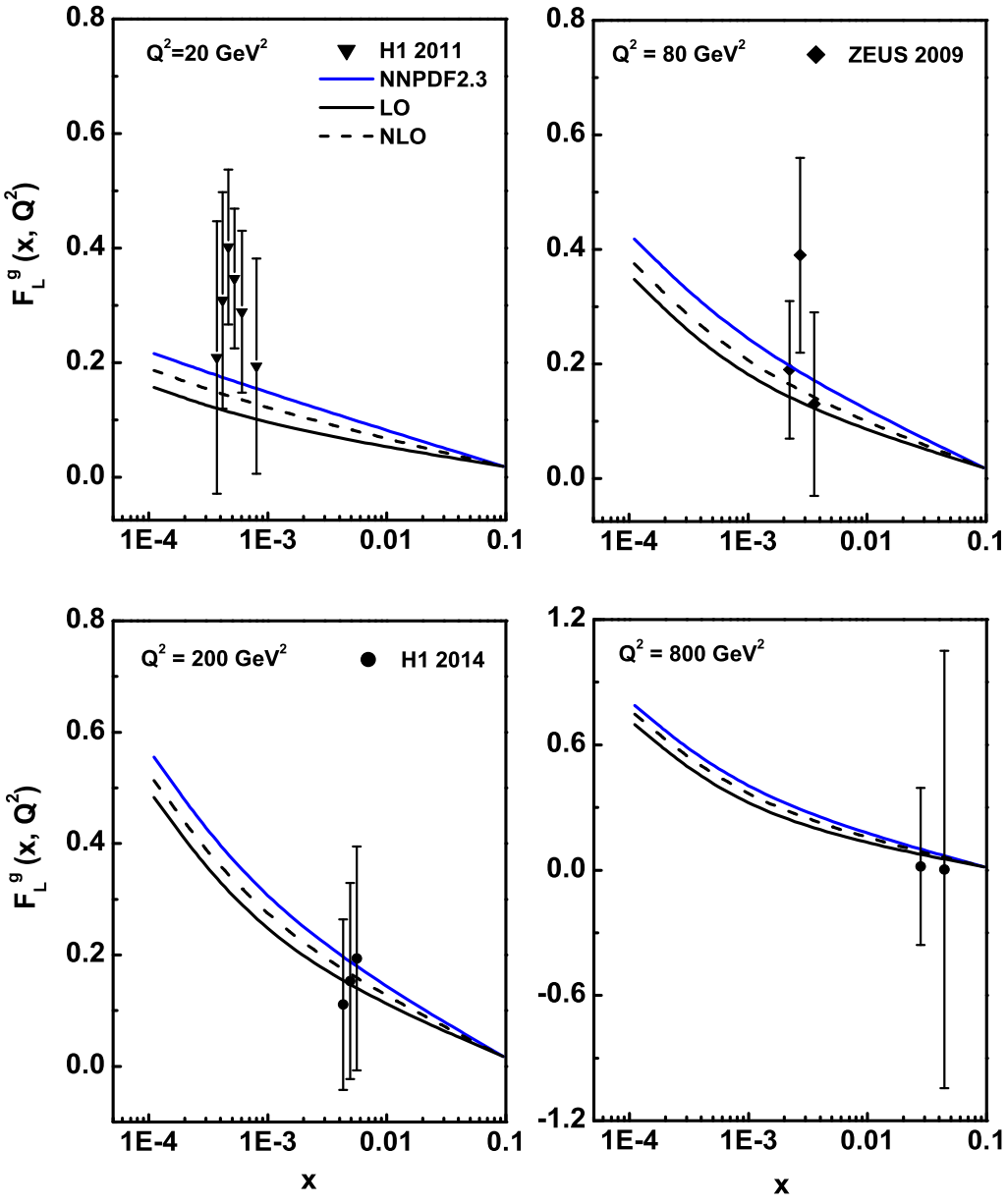

Figure 2.7: x-evolution results of F_L^g structure function up to NLO using Taylor expansion method in comparison with the H1, ZEUS data and the theoretical prediction of NNPDF2.3.

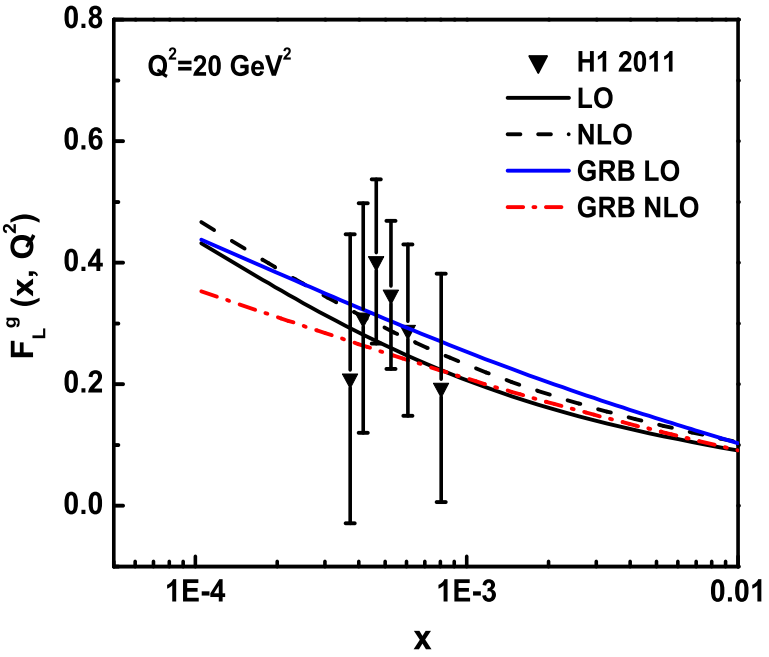

Figure 2.8: x-evolution results of F_L^g structure function up to NLO using Taylor expansion method in comparison with the H1 data and the theoretical prediction of Boroun et al. (GRB)

with data and related fits. In all the cases, the difference between different orders become less as the energy scale increases, which lies within the framework of pQCD i.e., running coupling constant becomes smaller as the energy value increases.

We have also presented a comparison of our results with the results reported in a recent paper by Boroun et al. where they have calculated the gluon dominating F_L structure function using Laguerre polynomials method [13]. Figure 2.8 shows the comparison of the results. Our results shows good agreement with the results of Boroun et al. In both the cases, the structure function increases towards small values of x as expected from QCD. Both the results does not show exactly the same behaviour as the methods for evaluating the structure function in both the cases are different, in our

case we have used 'Taylor expansion method' and they have used 'Laguerre polynomials method'.

2.3 Conclusions

In this chapter, we have obtained an analytical solution of evolution equation for gluon dominating longitudinal structure function F_L^g up to NNLO using the Taylor series expansion method. The solutions of the evolution equation provide the expressions for t- and x-evolution of F_L^g structure function. With the help of these expression, we have calculated the evolutions of F_L^g structure function by considering the input distributions from model fit and theoretical predictions of different parameterizations. Here, for the calculation of t- and x-evolution of F_L^g structure function we consider two numerical parameters T_0 and T_1. This method is simple one and less time consuming on the numerical calculations with less number of numerical parameters compared to the other methods where several parameters are included in the input function [38]. So, this method may be a viable alternative to other methods. To confirm the validity of our calculations, we have compared our results with recent experimental data. To show that in spite of the large error bars of the experimental data, our results are in good agreement with the data, we have compared our results with the results of model fit and parameterizations. The variation of F_L^g structure function with x and Q^2 shows similar nature with the H1, ZEUS experimental data as well as the results of DL model and theoretical predictions of MSTW08, CT10, ABM11 and NNPDF2.3. At small-x, our results show that the longitudinal structure function F_L^g increases with the increasing values of Q^2 and it also increases with the decreasing values os x as expected from QCD. As in our given range of x, the gluon contribution to the structure function is dominant one, so we can conclude in general that the gluon contribution to the longitudinal structure function increases with the values of Q^2 and it also increases

with the decreasing values of x.

References

[1] Aaron, F. D., et al. Measurement of the inclusive $e^{\pm}p$ scattering cross section at high inelasticity y and of the structure function F_L, *Eur. Phys. J. C.* **71** (3), 1579-1–50, 2011.

[2] Adloff, C., et al. Deep-inelastic inclusive *ep* scattering at low x and a determination of α_s, *Eur. Phys. J. C.* **21** (1), 33–61, 2001.

[3] Pardos, C. D. *Studies for the direct measurement of the proton structure function F_L with the H1 detector at HERA*, Ph.D. thesis, DESY, Zeuthen, Germany, 2007.

[4] Piec, S. *Measurement of the Proton Structure Function F_L with the H1 Detector at HERA*, Ph.D. thesis, Humboldt University of Berlin, Germany, 2009.

[5] Andreev, V., et al. Measurement of Inclusive *ep* Cross Sections at High Q^2 at $\sqrt{s} = 225$ and $252GeV$ and of the Longitudinal Proton Structure Function F_L at HERA, *Eur. Phys. J. C* **74** (4), 2814-1–26, 2014.

[6] Chekanov, S., et al. Measurement of the longitudinal proton structure function at HERA, *Phys. Lett. B* **682** (1), 8–22, 2009.

[7] Donnachie, A. and Landshoff, P. V. The protons gluon distribution, *Phys. Lett. B* **550** (3-4), 160–165, 2002.

[8] Martin, A. D., et al. Parton distributions for the LHC, *Eur. Phys. J. C* **63** (2), 189–285, 2009.

[9] Hung-Liang, Lai., et al. New parton distributions for collider physics, *Phys. Rev. D* **82** (7), 074024-1–24, 2010.

[10] Alekhin, S., Blemlein, J. and Moch, S. The ABM parton distributions tuned to LHC data, *Phys. Rev. D* **89** (5), 054028-1–21, 2014.

[11] Ball, R. D., et al. Parton distributions with LHC data, *Nucl. Phys. B* **867** (2), 244–289, 2013.

[12] Forte, S., et al. Heavy quarks in deep-inelastic scattering, *Nucl. Phys. B* **834** (1-2), 116–162, 2010.

[13] Rezaei, B. and Boroun, G. R. Analytical solution of the longitudinal structure function F_L in the leading and next-to-leading-order analysis at low x with respect to Laguerre polynomials method, *Nucl. Phys. A* **857** (1), 42–47, 2011.

[14] Cooper-Sarkar, A. M., et al. Measurement of the longitudinal structure function and the small x gluon density of the proton, *Z. Phys. C* **39** (2), 281–290, 1988.

[15] Moch, S. and Vogt, A. Threshold resummation of the structure function F_L, *J. High Energy Phys.* **2009** (04), 081-1–11, 2009.

[16] Kazakov, D. I., et al. Complete Quartic α_s^2 correction to the deep-inelastic longitudinal structure function F_L in QCD, *Phys. Rev. Lett.* **65** (13), 1535–1538, 1990.

[17] Guillen, J. S., et al. Next-to-leading order analysis of the deep inelastic $R = \sigma_L/\sigma_T$, *Nucl. Phys. B* **353** (2) 337–345, 1991.

[18] Moch, S., Vermaseren, J. A. M. and Vogt, A. The longitudinal structure function at the third order, *Phys. Lett. B* **606** (1-2), 123–129, 2005.

[19] Vermaseren, J. A. M., Vogt, A. and Moch, S. The third-order QCD corrections to deep-inelastic scattering by photon exchange, *Nucl. Phys. B* **724** (1-2), 3–182, 2005.

[20] Abbott, L. F., Atwood, W. B. and Barnett, R. M. Quantum-chromodynamic analysis of eN deep-inelastic scattering data, *Phys. Rev. D* **22** (3), 582–593, 1980.

[21] Furmanski, W. and Petronzio, R. Lepton-hadron processes beyond leading order in quantum chromodynamics, *Z. Phys. C* **11** (4), 293–314, 1982.

[22] Baishya, R., Jamil, U. and Sarma, J. K. Evolution of spin-dependent structure functions from DGLAP equations in leading order and next to leading order, *Phys. Rev. D* **79** (3), 034030-1–6, 2009.

[23] Baishya, R. and Sarma, J. K. Semi numerical solution of non-singlet Dokshitzer-GribovLipatovAltarelliParisi evolution equation up to next-to-next-to-leading order at small x, *Eur. Phys. J. C* **60** (4), 585–591, 2009.

[24] Sneddon, I. *Elements of Partial Differential Equations*, McGraw- Hill, New York, 1957.

[25] Sarma, J. K., Choudhury, D. K. and Medhi, G. K. x-distribution of deuteron structure function at low-x, *Phys. Lett. B* **403** (1-2), 139–144, 1997.

[26] Sarma, J. K. and Das, B. t evolutions of structure functions at low-x, *Phys. Lett. B* **304** (3-4), 323–328, 1993.

[27] Martin, A. D., et al. MRST2001: partons and α_S from precise deep inelastic scattering and Tevatron jet data, *Eur. Phys. J. C* **23** (1), 73–87, 2002.

[28] Martin, A. D., et al. Physical gluons and high-E_T jets, *Phys. Lett. B* **604** (1-2), 61–68, 2004.

[29] Martin, A. D., et al. Update of parton distributions at NNLO, *Phys. Lett. B* **652** (5-6), 292–299, 2007.

[30] Nadolsky, P. M., et al. Implications of CTEQ global analysis for collider observables, *Phys. Rev. D* **78** (1), 013004-1–21, 2008.

[31] Pumplin, J., et al. Collider inclusive jet data and the gluon distribution, *Phys. Rev. D* **80** (1), 014019-1–16, 2009.

[32] Aaron, F. D., et al. Combined measurement and QCD analysis of the inclusive $e\pm p$ scattering cross sections at HERA, *J. High Energy Phys.* **2010** (1), 109-1–63, 2010.

[33] Glazov, S. Measurement of DIS Cross Section at HERA, *Braz. J. Phys.* **37** (2C), 793–797, 2007.

[34] Kwiecinski, J., et al. Parton distributions at small x, *Phys. Rev. D* **42** (11), 3645–3659, 1990.

[35] Nematollahi, H., Yazdanpanah, M. M. and Mirjalili, A. NNLO longitudinal proton structure function, based on the modified χQM, *Mod. Phys. Lett. A* **27** (31),1250179-1-11 ,2012.

[36] Boroun, G. R. and Rezaei, B. Analysis of the proton longitudinal structure function from the gluon distribution function, *Eur. Phys. J. C* **72** (11), 2221-1-5, 2012.

[37] Devee, M., Baishya, R. and Sarma, J. K. Evolution of singlet structure functions from DGLAP equation at next-to-next-to-leading order at small-x, *Eur. Phys. J. C* **72** (6), 2036-1-11, 2012.

[38] Gluck, M., Reya, E. and Vogt, A. Dynamical Parton Distributions of the Proton and Small-x Physics, *Z. Phys. C* **67** (3), 433–447, 1995. □